INTERFACE

rsif.royalsocietypublishing.org

Research

Cite this article: Huang Y, Wang Y, Sun L, Agrawal R, Zhang M. 2015 Sundew adhesive: a naturally occurring hydrogel. *J. R. Soc. Interface* **12**: 20150226.
http://dx.doi.org/10.1098/rsif.2015.0226

Received: 12 March 2015
Accepted: 16 April 2015

Subject Areas:
bioengineering, biomaterials, nanotechnology

Keywords:
sundew adhesive, nano-network, naturally occurring hydrogel, tissue engineering

Author for correspondence:
Mingjun Zhang
e-mail: zhang.4882@osu.edu

Electronic supplementary material is available at http://dx.doi.org/10.1098/rsif.2015.0226 or via http://rsif.royalsocietypublishing.org.

THE ROYAL SOCIETY PUBLISHING

Sundew adhesive: a naturally occurring hydrogel

Yujian Huang[1,2,3], Yongzhong Wang[1,2,3], Leming Sun[1,2,3], Richa Agrawal[4] and Mingjun Zhang[1,2,3]

[1]Department of Biomedical Engineering, College of Engineering, [2]Dorothy M. Davis Heart and Lung Research Institute, Wexner Medical Center, [3]Interdisciplinary Biophysics Graduate Program, and [4]Department of Chemistry & Biochemistry, College of Arts and Sciences, The Ohio State University, Columbus, OH 43210, USA

Bioadhesives have drawn increasing interest in recent years, owing to their eco-friendly, biocompatible and biodegradable nature. As a typical bioadhesive, sticky exudate observed on the stalked glands of sundew plants aids in the capture of insects and this viscoelastic adhesive has triggered extensive interests in revealing the implied adhesion mechanisms. Despite the significant progress that has been made, the structural traits of the sundew adhesive, especially the morphological characteristics in nanoscale, which may give rise to the viscous and elastic properties of this mucilage, remain unclear. Here, we show that the sundew adhesive is a naturally occurring hydrogel, consisting of nano-network architectures assembled with polysaccharides. The assembly process of the polysaccharides in this hydrogel is proposed to be driven by electrostatic interactions mediated with divalent cations. Negatively charged nanoparticles, with an average diameter of 231.9 ± 14.8 nm, are also obtained from this hydrogel and these nanoparticles are presumed to exert vital roles in the assembly of the nano-networks. Further characterization via atomic force microscopy indicates that the stretching deformation of the sundew adhesive is associated with the flexibility of its fibrous architectures. It is also observed that the adhesion strength of the sundew adhesive is susceptible to low temperatures. Both elasticity and adhesion strength of the sundew adhesive reduce in response to lowering the ambient temperature. The feasibility of applying sundew adhesive for tissue engineering is subsequently explored in this study. Results show that the fibrous scaffolds obtained from sundew adhesive are capable of increasing the adhesion of multiple types of cells, including fibroblast cells and smooth muscle cells, a property that results from the enhanced adsorption of serum proteins. In addition, in light of the weak cytotoxic activity exhibited by these scaffolds towards a variety of mammal cells, evidence is sufficient to propose that sundew adhesive is a promising nanomaterial worth further exploitation in the field of tissue engineering.

1. Introduction

Sundew (*Drosera* spp.), one of the intriguing carnivorous plants, has fascinated scientists owing to its peculiar lifestyle. Small prey, such as insects, are attracted, entrapped, digested and absorbed by sundew plants to fulfil their nutritional needs of minerals, especially nitrogen and phosphorus [1,2]. To accomplish relevant physiological functions without compromising the photosynthetic efficiency, two distinct glands are differentiated, appearing on the leaves of sundew, i.e. the sessile gland, which secretes digestive enzymes, and the stalked gland, which exudes aqueous mucilage at the head [1,3]. The sticky exudate exists in the form of tiny droplets at the tips of the stalked glands, glittering in the sun like dewdrops, to attract prey and to restrict them from escaping (figure 1*a*) [1,4].

The adhesive observed on the stalked glands of sundew is viscoelastic, as evidenced in previous mechanical studies [1,3]. The rheological characteristics of the sundew adhesive, involving high fluid viscosity, capillary thinning and extensional viscoelasticity, have been investigated by newly developed interferometry-based microrheometer and capillary thinning microrheometer [3].

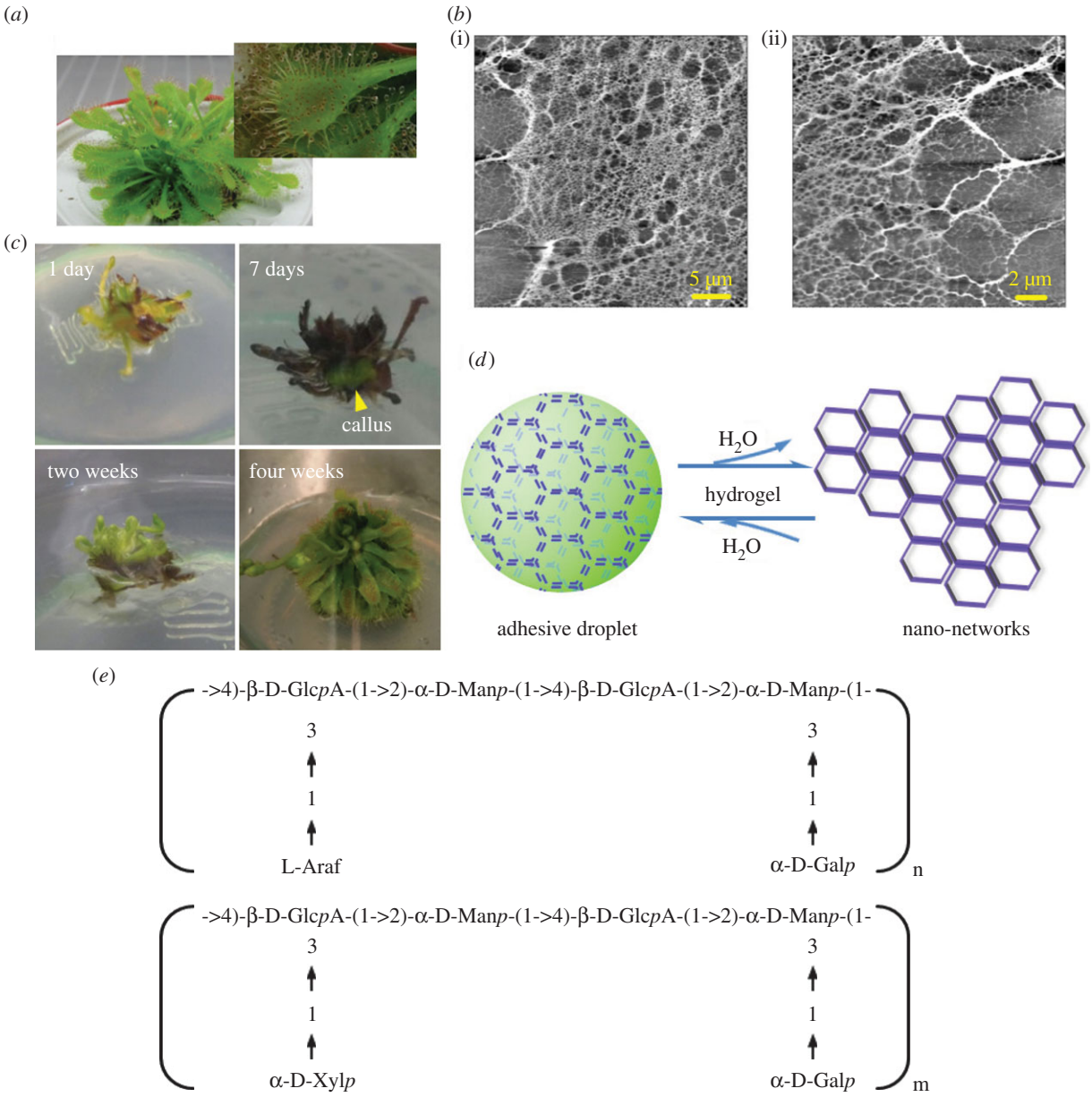

Figure 1. A naturally occurring hydrogel secreted by sundew plants. (*a*) Images of sundew plant (*D. spatulata*) and the mucilage secreted from the stalked glands on the leaves of sundew plant. (*b*) AFM images of nano-network architectures obtained in the sundew adhesive. Scale bars represent 5 µm (i) and 2 µm (ii). (*c*) *In vitro* tissue culture of sundew plants. Yellow arrow indicates the formed callus tissue. (*d*) A schematic drawing of the sundew adhesive, which is considered as a naturally occurring hydrogel. (*e*) Typical glycosyl composition and linkages of the polysaccharides obtained in sundew adhesive. (Online version in colour.)

Within the genus *Drosera*, chemical ingredients for the mucilage secreted by dissimilar species are homologous [1,3,5–7]. In most cases, the sticky liquid is composed of 4% (w/v) acidic polysaccharides with glycosyl backbones characterized by repeating dimers rich in glucuronic acid (Glc*p*A) and mannose (figure 1*e*) [1,3,8]. The ratios of monosaccharide residues existing on the side chains demonstrate a slight difference (figure 1*e*) [1,3]. Protein is not detected in the sundew adhesive and enzymes are secreted by the sessile glands only after stimulation by prey [1]. In terms of the inorganic ions, cations are abundantly observed in this viscoelastic adhesive and the divalent ones, including Mg^{2+} and Ca^{2+}, are proposed to be involved in the neutralization of the uronic acidic residues in the sundew adhesive, via electrostatic interactions at pH 5.0 under natural conditions [3,8]. In *Drosera capensis*, 22 mM Ca^{2+}, 19 mM Mg^{2+}, 0.9 mM K^{+} and 0.2 mM Na^{+} are detected in the secreted mucilage as measured by atom absorption spectrophotometry [1,8].

Macroscopic morphological characteristics of the sundew adhesive have been investigated using cryo-scanning electron microscopy in the earlier studies [1,9]. It has been observed that hollow pores are densely distributed on the surface of the mucilage, arising from the partial sublimation of frozen water in the adhesive during the cryo-stage [9]. The dispersed distribution of these tiny pores suggests the presence of framework structures in the sundew adhesive, and the water is presumably retained in these three-dimensional architectures. A subsequent study using atomic force microscopy (AFM) verifies the hypothetical framework structures in the sundew adhesive, and further indicates that the nano-network architectures observed in the sundew adhesive are assembled by polysaccharides [10,11]. However, despite the progress made in understanding the structural characteristics of sundew adhesive, it remains elusive as to whether structural traits of the sundew adhesive, especially the morphological features in nanoscale, are associated with the viscoelastic property of this adhesive.

Sundew adhesive has been extensively exploited in the pharmaceutical and food industry, owing to its biocompatibility and mildly antibiotic activity [1,12]. Apart from that, the nano-network architectures observed in sundew adhesive have been further developed as scaffolds that facilitate the adhesion of both MC3T3-E1 mouse pre-osteoblastic cells and PC12 neuronal cells, and favour the differentiation of PC12 neuronal cells [10,11]. Even though the underlying mechanisms for the enhanced cell adhesion are still unclear, these beneficial properties suggest that sundew adhesive has great potential as an alternative to traditionally synthetic scaffolds for tissue engineering, in particular, for wound healing and therapeutic angiogenesis [10,11].

Herein, we investigate the physico-chemical properties of the sundew adhesive, explicate the structural traits that result in its viscoelastic behaviour and propose the self-assembly mechanisms for the polysaccharides contained in this adhesive. This study also reveals that sundew adhesive, a naturally occurring hydrogel, may be extensively exploited as biocompatible scaffolds for tissue engineering in the future.

2. Material and methods

2.1. Materials and reagents

Drosera capensis and Drosera spatulata were obtained from local nurseries (Columbus, OH, USA). Mouse aortic smooth muscle cells (MSMCs) and rat aortic smooth muscle cells (RSMCs) were prepared from explants of excised aortas of mice or rats as described previously [13]. MC3T3-E1 mouse pre-osteoblastic cells (CRL-2593) and NIH3T3 mouse embryo fibroblast cells (CRL-1658) were obtained from the American Type Culture Collection (Manassas, VA, USA). Fetal bovine serum, minimum essential medium alpha (MEM-α) and Dulbecco's modified Eagle's medium (DMEM) were purchased from Mediatech (Manassas, VA, USA). Penicillin (10 000 units ml^{-1})–streptomycin (10 000 μg ml^{-1}) solution was obtained from MP Biomedicals (Solon, OH, USA). Hoechst 33342 was purchased from Invitrogen Life Technologies (Grand Island, NY, USA). Other chemicals were ordered from Sigma (St Louis, MO, USA). All the water used for characterization and chemical identification was prepared using an ultrapure water system (LaboStar^{TM} TWF UV7, Siemens, MA, USA).

2.2. *In vitro* cultivation of *Drosera capensis* and *Drosera spatulata*

Leaves obtained from the mature sundew plants were used as explants, which were surface-sterilized by 10% (w/v) sodium hypochlorite for 10 min and then rinsed with aseptic water three times. Sterilized explants were placed onto half-strength Murashige & Skoog medium containing 30 g l sucrose and 1 mg l kinetin. After bud induction for two weeks, the explants were subsequently cultured onto successive medium consisting of half-strength Murashige & Skoog with 30 g l sucrose, 1 mg l potassium salt of indole-3-butyric acid, and 1 mg l kinetin, in order to initiate roots and shoots. All media were adjusted to pH 5.8 prior to sterilizing and then solidified with 0.7% (w/v) agar. The explants were cultured in vessels at 25 ± 2°C, with a 16 L : 8 D photoperiod. Plantlets were removed from the vessels after one month of culture and transplanted into pots with a mixture of sterilized sand : peat (1 : 2, v/v). The pots were enclosed within plastic bags for 5 days. After the hardening-off process was accomplished, the plantlets were eventually cultured in a plant incubator. Mucilage secreted from the stalked glands of the *in vitro* cultured sundew plants was collected using a pipette equipped with wide-bore pipet tips (VWR Scientific Products, Westchester, PA, USA). The obtained sundew adhesive was used for characterization rapidly, to avoid the influence of water evaporation on its physico-chemical properties.

2.3. Characterization of sundew adhesive

Dried sundew adhesive was visualized using a MFP-3D AFM (Asylum Research, Santa Barbara, CA, USA). Ten microlitres of the sundew adhesive was dropped onto the surface of a coverslip, followed by air-drying overnight at room temperature. Nano-networks of sundew adhesive were scanned in tapping mode at room temperature, using an ACTA-SS probe (Applied NanoStructures, Inc., Santa Clara, CA, USA). The control system used for this platform was IGOR Pro and the sample was scanned at a rate of 0.5 ln s^{-1}, with three scan ranges, i.e. 40 × 40 μm, 20 × 20 μm and 5 × 5 μm. In order to study the morphological features in detail, sundew adhesive was suspended in water and the suspension was ultrasonicated in an ice-water bath (Aquasonic model 250D water bath, VWR Scientific Products) for 1 h. The resultant solution was filtered through a 0.22-μm syringe filter (Millipore, Bedford, MA, USA) to eliminate bulky debris. Twenty microlitres of the filtrate was placed onto a coverslip and visualized using AFM after air-drying overnight at room temperature. Mean size, size distribution and zeta potential of the suspended nanoparticles were characterized by dynamic light scattering (DLS) and electrophoretic light scattering (ELS) at room temperature, using a Malvern Zetasizer, Nano ZS (Malvern Instruments Ltd, Worcestershire, UK). Meanwhile, the concentration of proteins in the sundew adhesive was quantitatively determined using the BCA protein assay (Pierce, Rockford, IL, USA) following the manufacturer's instructions. All measurements were performed in triplicate ($n = 3$).

2.4. X-ray photoelectron spectroscopic measurements

The functional groups of sundew adhesive, as well as other typical polysaccharides, including chitosan, cellulose, alginate and pectin, were characterized by X-ray photoelectron spectroscopic (XPS) measurements using a PHI 3056 XPS spectrometer (Physical Electronics, Inc., Chanhassen, MN, USA) with an Al Kα anode source, operated at 350 W. Dissolved samples were placed onto the coverslips, followed by air-drying overnight at room temperature. A low-resolution scan was carried out with 93.5 eV pass energy, 0.5 eV energy step. A high-resolution scan was performed with pass energy of 23.5 eV, an energy step of 0.05 eV, and 70 repeats were done to improve the ratio of signal to noise. The measurement order was C 1 s, N 1 s and S 2 s. Binding energy spectra were calibrated via designating the aliphatic carbon signal to 284.8 eV in response to changes. Recorded spectra of each sample were analysed, in comparison to those of the bare coverslip.

2.5. High-speed camera measurements

For real-time observation of the viscoelastic adhesion of sundew adhesive, a Powerview HS-650 (TSI, Inc., Shoreview, MN, USA) high-speed camera system, with a Sigma 18–200 mm lens, was used to capture the adhesion pattern of the sundew adhesive in excess of 800 fps. A Lumina FO-150 fibre-optic light source was used associated with the camera system. For such purpose, needles or coverslips were used as substrates to contact the *in situ* secreted mucilage on the leaves of the sundew plants. The overall process, involving the approaching and the detaching, was recorded. The obtained images were analysed and combined to create videos using ImageJ.

2.6. Contact angle measurements

The contact angle (CA) of sundew adhesive was analysed in comparison to that of the water. Twenty microlitres of the

sundew adhesive or water was dropped onto the siliconized glass slides (Atlantic SciTech Group, Inc., Linden, NJ, USA), and the CAs for each sample were recorded at room temperature. Apart from that, the water CAs of different hydrophobic substrates modified with sundew adhesive were also evaluated and compared to those of the bare substrates. For this purpose, 5 µl of the sundew adhesive was coated onto the siliconized glass slides and polystyrene slides (VWR Scientific Products), respectively. After air-drying overnight at room temperature, 20 µl of water was dropped onto the adhesive-modified surfaces and the CAs for each sample were measured at room temperature. The measurements for each sample were performed in triplicate ($n = 3$).

2.7. Atomic force microscopy force curve measurements

Force curve measurements using AFM were carried out according to the methods that have been developed for characterizing other types of bioadhesives in earlier studies [14–19]. For this purpose, 20 µl of sundew adhesive was collected and treated at −80°C, −20°C and room temperature (20°C) for 2 h, respectively. Each sample was then dropped onto the coverslips and the force curves were obtained using the same MFP-3D AFM (Asylum Research) as mentioned above, via probing the adhesive in the *Z*-direction using the cantilever tips, i.e. force mode. In this comparative study, various samples tested on the coverslips were considered to have similar thicknesses at the same concentration and volume. Silicon probes (Nanosensors™, Neuchatel, Switzerland) with a spring constant of 0.32 ± 0.01 N m^{-1} were used and the force curve measurements scanned in the *Z*-direction at a rate of 3 µm s^{-1} with constant applied load. Output data were obtained as the deflection of the cantilever tips (volts) versus piezo displacement (*Z*, nm), and the raw data were converted to force (nN) versus displacement (µm) curves automatically with the associated control program (IGOR Pro, WaveMetrics, Inc., Portland, OR, USA) according to the principles described in previous studies [14,16,20]. Briefly, for a small deflection x, the force (F) on the cantilever is defined by Hooke's Law, $F = kx$, where k is the spring constant of the cantilever [16]. Adhesion strength (N m^{-1}), which is defined as the force/radius of the cantilever tip [14,16], was calculated according to the retraction portion of the obtained force curves. Here, the tip had a radius of 0.1 µm [16,21]. Force curve measurements conducted in this study were accomplished in several days, using new cantilevers whose spring constant values were calibrated as outlined previously [22,23]. In addition to sundew adhesive, force curves were taken on bare coverslips to check whether the cantilever tip had been contaminated or not, after each test. Force curve measurements for each sample were performed in triplicate ($n = 3$).

2.8. MTT assay

The MTT (3-[4, 5-dimethylthiazol-2-yl]-2, 5-diphenyl tetrazolium bromide) assay was carried out to assess the cytotoxicity of sundew adhesive, according to a method described earlier [24,25]. Briefly, four types of cells, including MC3T3, NIH3T3, MSMC and RSMC, were seeded into 96-well tissue culture plates (TCPs) at a concentration of 1×10^4 cells per well. MC3T3 mouse pre-osteoblastic cells were cultured in MEM-α supplemented with 10% fetal bovine serum and 1% penicillin–streptomycin; NIH3T3 mouse embryo fibroblast cells were cultured in DMEM supplemented with 10% calf serum and 1% penicillin–streptomycin; MSMCs and RSMCs were cultured in DMEM supplemented with 10% fetal bovine serum and 1% penicillin–streptomycin. Serial dilutions of sundew adhesive were added into the wells, and the TCPs were incubated at 37°C in 5% CO_2 for 48 h. Ten microlitres of MTT stock solution (5 mg ml^{-1} in phosphate-buffered saline [PBS], pH 7.4) was then added into each well, and the TCPs were incubated at 37°C for another 4 h. The medium was then removed and 100 µl of DMSO was added into each well to solubilize the dye. The optical density at 570 nm was measured by a microplate reader (Bio-Tek µQuant). The cell viabilities were determined in comparison to the untreated group.

2.9. Cell proliferation measurements

Two microlitres of sundew adhesive was uniformly coated into each well of the 48-well TCPs. For the proliferation assay, four types of cells (MC3T3, NIH3T3, MSMC and RSMC) were seeded into the TCPs at a concentration of 1×10^4 cells per well and incubated at 37°C in 5% CO_2. The medium was changed every 2 days and the MTT assay was performed at day 1, 3, 5 and 7, to measure the optical densities at 570 nm. The same proliferation assay was also performed on a bare 48-well plate as a control.

2.10. Cell adhesion assay

To test the cell adhesion properties of sundew adhesive, 2 µl of sundew adhesive was uniformly coated onto the coverslips which were then placed into six-well TCPs. Four types of cells (MC3T3, NIH3T3, MSMC and RSMC) were seeded into the TCPs at a concentration of 1.5×10^5 cells per well and incubated at 37°C in 5% CO_2. After 4 h incubation, the coverslips were rinsed with PBS three times to remove non-adherent cells. The adherent cells on the coverslips were then fixed with 8% formaldehyde for 30 min and stained with nucleus-specific dye Hoechst 33342 (4 µM) for 30 min, followed by rinsing with PBS three times, prior to visualizing with a FluoView FV1000 confocal microscopy (Olympus, Japan). Ten random fields were chosen from the obtained image, and the adherent cells in each field were counted by ImageJ. Cell adhesion assays were performed in both serum-free and serum-containing media. Cell adhesion tests for each sample were performed in triplicate ($n = 3$).

2.11. Statistical analysis

Data are expressed as mean ± s.d. Statistical significance was determined using a two-tailed Student's *t*-test. $P < 0.05$ was considered to be statistically significant.

3. Results and discussion

3.1. Naturally occurring hydrogel secreted by sundew

The adhesive secreted by the stalked glands on the leaves of sundew was *in situ* gathered and characterized using AFM. As shown in figure 1*b*, tight-knit nano-networks, with a comparatively wide distribution of pore sizes, ranging from micro- to nano-scales, were observed in the dried sundew adhesive. It was also observed that the formed nano-networks are tightly assembled by the cross-linking of nanofibres (figure 1*b*). Given that the dried sundew adhesive is highly hygroscopic and shows a gel-like consistency, as evidenced in the earlier studies [1,8], it seems reasonable to assume that sundew adhesive is a naturally occurring hydrogel (figure 1*d*). By definition, hydrogels are water-swollen, polymeric and cross-linked networks capable of imbibing and retaining a significant fraction of aqueous phase within their three-dimensional configurations, rather than being dissolved in surrounding water [26,27]. In this respect, as the previous studies have indicated that the fibrous structure of the nano-networks obtained from sundew adhesive consists of polysaccharides [10,11], which are commonly regarded as biopolymers [28,29], and in light of the fact that even though water occupies a proportion of up to 96%

(w/w) in sundew adhesive [1,8], the dissolving rate of sundew adhesive in surrounding aqueous environment is exceedingly slow [8], evidence is sufficient to support the proposed concept that the sundew adhesive is a naturally occurring hydrogel. Typically, hydrogels have an excellent capacity to absorb water, a property arising from the presence of bulk hydrophilic groups in polymers, including -OH, -$CONH_2$, -CONH- and many others [27]. Likewise, the hygroscopic feature of sundew adhesive is attributed to the abundant -OH groups existing on the polysaccharide-rich architectures. Polysaccharides act as frameworks in sundew adhesive, retaining the aqueous phase and sustaining the overall structure. In turn water acts as a dispersive medium to stabilize these biopolymers. It is noteworthy that the water occupies the majority of the total amount in this naturally occurring hydrogel [1,8], making it an excellent candidate for biomaterials used in tissue engineering. Clinical applications such as minimally-invasive surgery or localized therapy could potentially make use of this hydrogel, as the ratio of water is a crucial factor to estimate the injectability of polysaccharide-rich hydrogels [30,31].

Given that the amount of mucilage provided by an individual sundew plant is limited, a platform was developed for *in vitro* culture of *D. capensis* and *D. spatulata* in order to obtain sufficient samples for this study (figure 1*c*). It was observed that callus appeared on the explants in approximately one week, in response to the induction of 1 mg l^{-1} cytokinin (kinetin). After one more week's cultivation for bud production, the explants were sub-cultured onto successive medium containing 1 mg l^{-1} potassium salt of indole-3-butyric acid and 1 mg l^{-1} kinetin to initiate the growth of shoots and roots. As shown in figure 1*c*, leaves and roots formed approximately two weeks later. The plantlets were then removed from the vessels, planted into pots and cultured in a plant incubator after the hardening-off procedure. Sticky exudate was obtained from the stalked glands of the *in vitro* cultured sundew plants after one month (figure 1*a*).

3.2. Functional groups aiding in the assembly of the nano-networks within sundew adhesive

The chemical elements and functional groups of sundew adhesive were characterized using XPS and compared to other types of polysaccharides, including cellulose, pectin, chitosan and alginate, in order to investigate the differences and to discuss the implied mechanisms that might result in the assembly of polysaccharides in sundew adhesive.

As shown in figure 2*a*, in general, all types of polysaccharides exhibited similar wide-scan photoelectron spectra, despite that N 1 s peaks were only partially detected. The N 1 s signals of chitosan and pectin are attributed to the presence of amino groups and *N*-acetyl groups. Further, a high-resolution scan indicated that nitrogen atoms also exist in the sundew adhesive (figure 2*c*), and the peak centred at 402.2 eV is assigned to the ammonium groups, which may result from the amidation of polysaccharides in the sundew adhesive. In order to substantiate that the N 1 s signal of sundew adhesive arises from the functional groups within the polysaccharides, instead of resulting from potential proteins, a BCA protein assay was performed to quantitatively determine the protein level in sundew adhesive. As expected, a proteinaceous signal was not detected in sundew adhesive, and this result is consistent with those of the earlier studies [1,8]. This supports the conclusion that the nitrogen atoms are located within the carbohydrate chains of sundew adhesive. C 1 s narrow-scan spectra of sundew adhesive were fitted into three Gaussian components, centred at 287.46, 289.13 and 290.74 eV, which are assigned to the C–O, C=O and O–C=O groups, respectively (figure 2*b*). The O–C=O groups are associated with the Glc*p*A residues existing in the glycosyl backbone of sundew adhesive. Sulfur was detected in *D. capensis* (figure 2*d*) and may exist in a form of ester sulfate in sundew adhesive, as proposed in the previous turbidimetric studies [1,8].

Pectin, alginate, as well as the polysaccharides in sundew adhesive are all capable of forming gel-like matrices [32–39]. In this respect, given that sundew adhesive exhibits functional groups that resemble those of pectin and alginate, as evidenced in the XPS study (figure 2*a*), it seems reasonable to presume that the polysaccharides in the sundew adhesive, pectin and alginate may show similarities in the gelation process. The gelation mechanisms for pectin and alginate have been well elucidated by an 'egg-box' model, which attributes the cross-linking of the polysaccharides to the electrostatic interactions among uronic acid residues, including galacturonic acids (Gal*p*A) and guluronic acids (Gul*p*A). This process is driven by the divalent cations, mainly calcium ions (figure 2*e*) [32,33,40]. As similar uronic acid residues, i.e. Glc*p*A, appear repeatedly in the glycosyl backbone of sundew adhesive [1,3], it is reasonable to assume that the assembly of the polysaccharides in sundew adhesive also results from the divalent cations-mediated cross-linking. This proposed assembly model is well supported by the results of the earlier studies, which conclude that the majority of the uronic acidic residues in sundew adhesive are neutralized by Ca^{2+} and Mg^{2+} ions [3,8]. In terms of the formed matrices, a previous transmission electron microscopic study has demonstrated a nano-network architecture formed by calcium alginate similar to the fibrous structures observed in sundew adhesive [41]. However, this architecture is loosely stitched and is not as tight-knit as that obtained in sundew adhesive, comparatively [41].

3.3. Nanoparticles observed in sundew adhesive

Compared with other types of polysaccharides in solution, sundew adhesive is exceptional in displaying a strong viscoelastic behaviour [1,3]. In general, physico-chemical characteristics are intimately relevant to the morphological features. In this respect, investigation of the structural traits aiding in the assembly of the nano-networks in sundew adhesive may allow us to elucidate the viscoelastic properties of this adhesive. Our previous study has shown that individual nanofibres in sundew adhesive may be linearly assembled by nano-sized organic particles [10], and this proposed concept provides an insight into the nano-network structures of sundew adhesive. In this study, further investigation was carried out via sonicating the sundew adhesive to break weak bonds among polysaccharides. As shown in figure 3*a*,*b*, abundant nanoparticles, with a mean diameter of 231.9 $\pm$ 14.8 nm and a broad range of size distribution (90% of the obtained nanoparticles were distributed in a size range of 91.3 to 458.7 nm in diameter), were observed in the resultant solution as measured by AFM and DLS. These nanoparticles showed a zeta potential of -23.9 ± 1.7 mV at neutral pH, and the negative charge of these nanoparticles presumably arises from the Glc*p*A residues that are distributed in the glycosyl backbone of the sundew adhesive

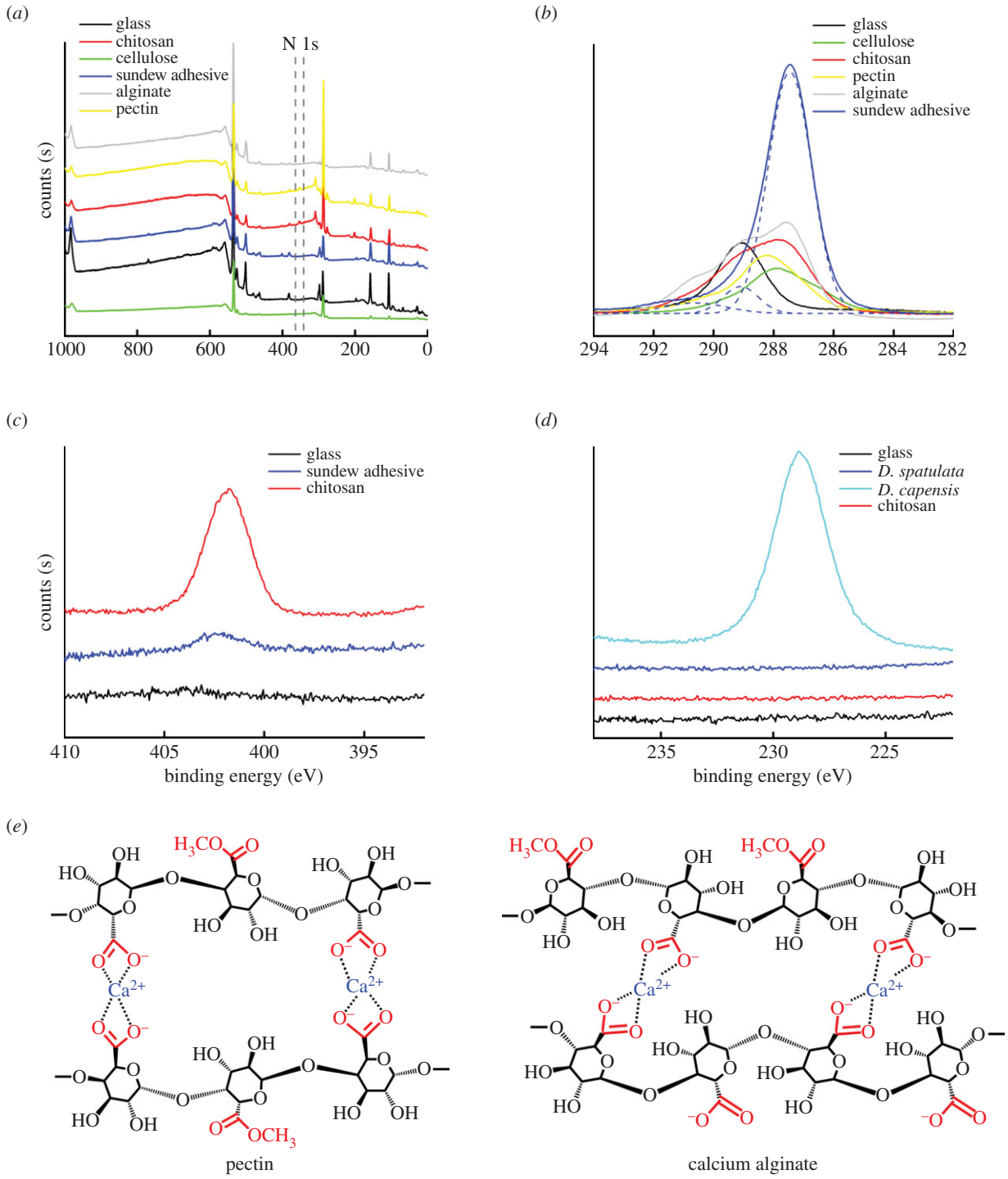

Figure 2. XPS measurements of sundew adhesive. (*a*) XPS wide spectra of sundew adhesive, chitosan, cellulose, alginate and pectin. (*b*) C 1 s narrow spectra of sundew adhesive, chitosan, cellulose, alginate and pectin. The C 1 s spectra of sundew adhesive were fitted into three Gaussian components, using 'Multi-peaks' function of Origin Pro 9.0. (*c*) N 1 s narrow spectra of sundew adhesive and chitosan. (*d*) S 2 s narrow spectra of chitosan and adhesive secreted by *D. capensis* and *D. spatulata*. (*e*) A schematic drawing of the proposed 'egg-box' model for pectin and calcium alginate. (Online version in colour.)

(figure 3*c*). It is well known that acidic polysaccharides are prone to forming spheroidal architectures in aqueous solution by means of calcium-mediated gelation. A typical instance is the Ca^{2+}-alginate nanoparticles formed via self-assembly in aqueous environments [42–45]. In light of this, given that divalent cations, i.e. Ca^{2+} and Mg^{2+}, also abundantly exist in the sundew adhesive [1,8], the nanoparticles observed in the sundew adhesive are presumably formed via electrostatic interactions among polysaccharides, driven by divalent cations. According to this proposed model, it seems reasonable to hypothesize that the size of the nanoparticles obtained from sundew adhesive may be associated with the length of the polysaccharide chains, the proportion of the uronic acid residues and the concentration of the divalent cations.

3.4. Structural traits giving rise to the viscoelastic behaviour of sundew adhesive

The mucilage secreted by sundew plants exhibits a viscoelastic property [1,3], allowing the plants to be capable of arresting and detaining insects [10]. To better observe the adhesion behaviour of this mucilage, needle and microscope coverslips were used as adherends to *in situ* contact the adhesive droplets secreted on the leaves of sundew plants

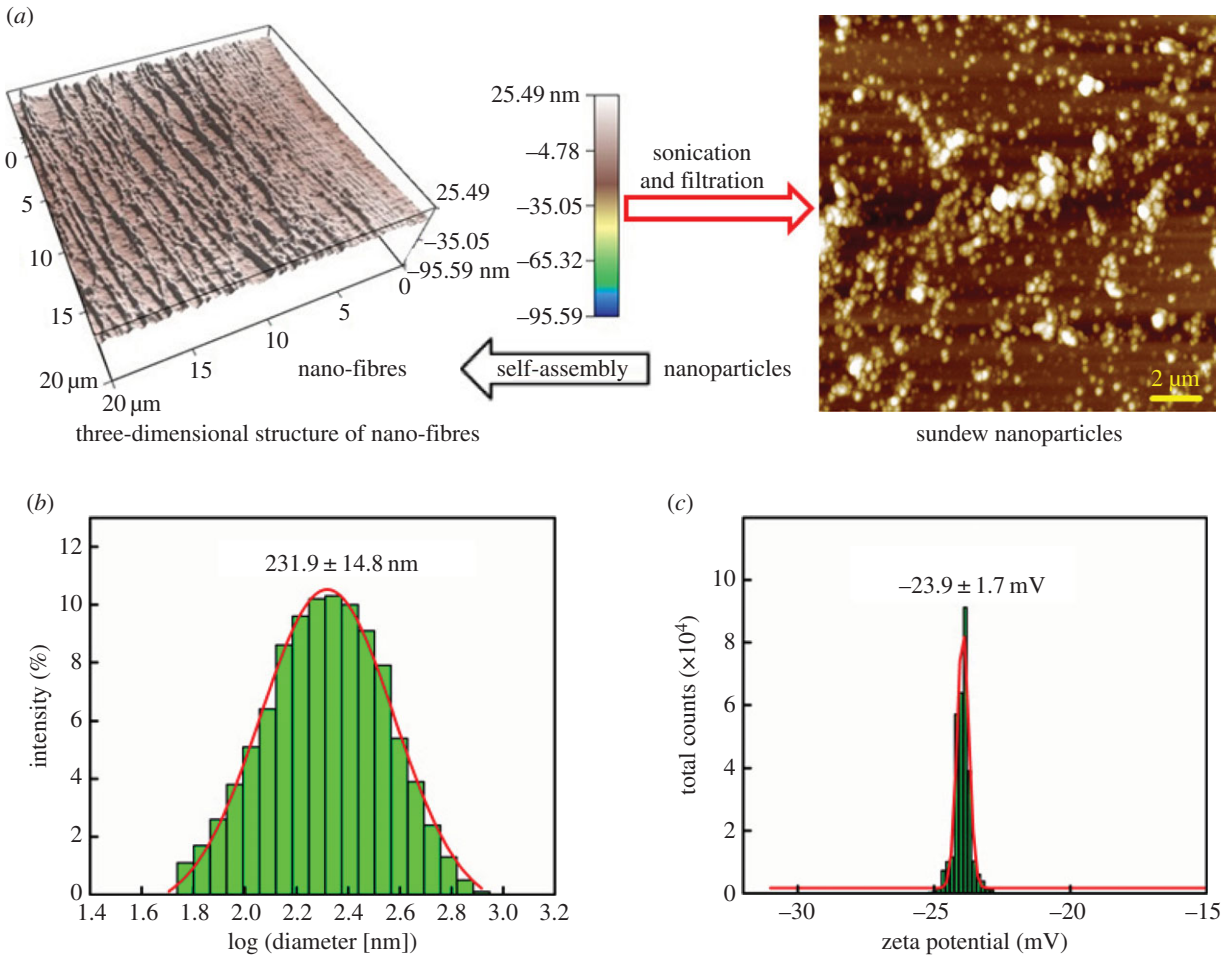

Figure 3. Nanoparticles obtained from the sundew adhesive. (*a*) AFM images of the nanofibres and the nanoparticles obtained in sundew adhesive. Left panel, external tensile force was applied on the sundew adhesive prior to the AFM measurements. Size for the left image is 20 × 20 μm and the scale bar for the right image represents 2 μm. (*b*,*c*) Mean size and zeta potential of the obtained nanoparticles characterized by DLS and ELS, respectively. The average size for the obtained nanoparticles was 231.9 ± 14.8 nm in diameter and the zeta potential was −23.9 ± 1.7 mV. (Online version in colour.)

(electronic supplementary material, videos S1, S2 and S3). The overall process, throughout the approaching and the detaching of the adherends, was captured by a high-speed camera system (Powerview HS-650). As shown in figure 4*a* and electronic supplementary material, video S1 and S2, it was observed that the sundew adhesive promptly formed a flat disc at the contact surface upon touching the coverslips, suggesting good wettability of this mucilage on the surface of glass slides. Rapid stretching deformation was observed in sundew adhesive while backward tensile force was applied on the adherends prone to dissociating the adhesive bonding, resulting in a spindly thread of mucilage that resists separation of the adherends. Although previous mechanical studies have advanced the understanding of this viscoelastic adhesive [3], the morphological characteristics of sundew adhesive, especially the structural traits in nanoscale, which give rise to the viscoelastic features, remain unclear. In the current study, an attempt was made to establish the correlation between structural traits and the physical properties. For such a purpose, the morphological variations of the nano-network architectures, in response to the stretching deformation of sundew adhesive, were examined using AFM. As shown in figure 4*b*, while a lateral tensile force was applied on the sundew adhesive, interestingly, the porous nano-networks were not scattered or fractured into pieces, but altered in appearance from an irregular polygon to a parallelogram-like shape along the direction of the exerted external force. This deformation suggests that the nano-networks within sundew adhesive are exceedingly flexible, aiding in buffering the external force which may impair the adhesive bonding, and presumably resulting in the viscoelastic property of the sundew adhesive.

Apart from the viscoelastic behaviour, the wettability of the sundew adhesive was also quantitatively evaluated by measuring the CAs. The values for $CA_{sundew\ adhesive}$ and CA_{water} on various substrates are listed in table 1. For the hydrophobic slides made of siliconized glass, the sundew adhesive exhibited a $CA_{sundew\ adhesive}$ of 46.8 ± 1.8° on the surface, whereas a CA_{water} of 82.7 ± 1.4° was observed on the same surface (table 1 and figure 4*c*), suggesting that better spreading is achieved by sundew adhesive on a hydrophobic surface as compared with water. In the case of the siliconized glass slides modified with dried sundew adhesive, the CA_{water} on the surface was approximately 1.5-fold lower than that on the bare siliconized glass, as shown in table 1 and figure 4*c*. This elevated hydrophilicity of siliconized glass slides presumably arises from the hygroscopic feature of sundew adhesive [8]. This result is further verified by measuring the CA_{water} on the polystyrene slides. As shown in table 1 and figure 4*c*, polystyrene slides modified with dried sundew adhesive showed approximately 1.3-fold lower CA_{water} on the surface, in comparison to bare slides. As polystyrene slides also display a hydrophobic surface, data here suggest that sundew adhesive is capable of

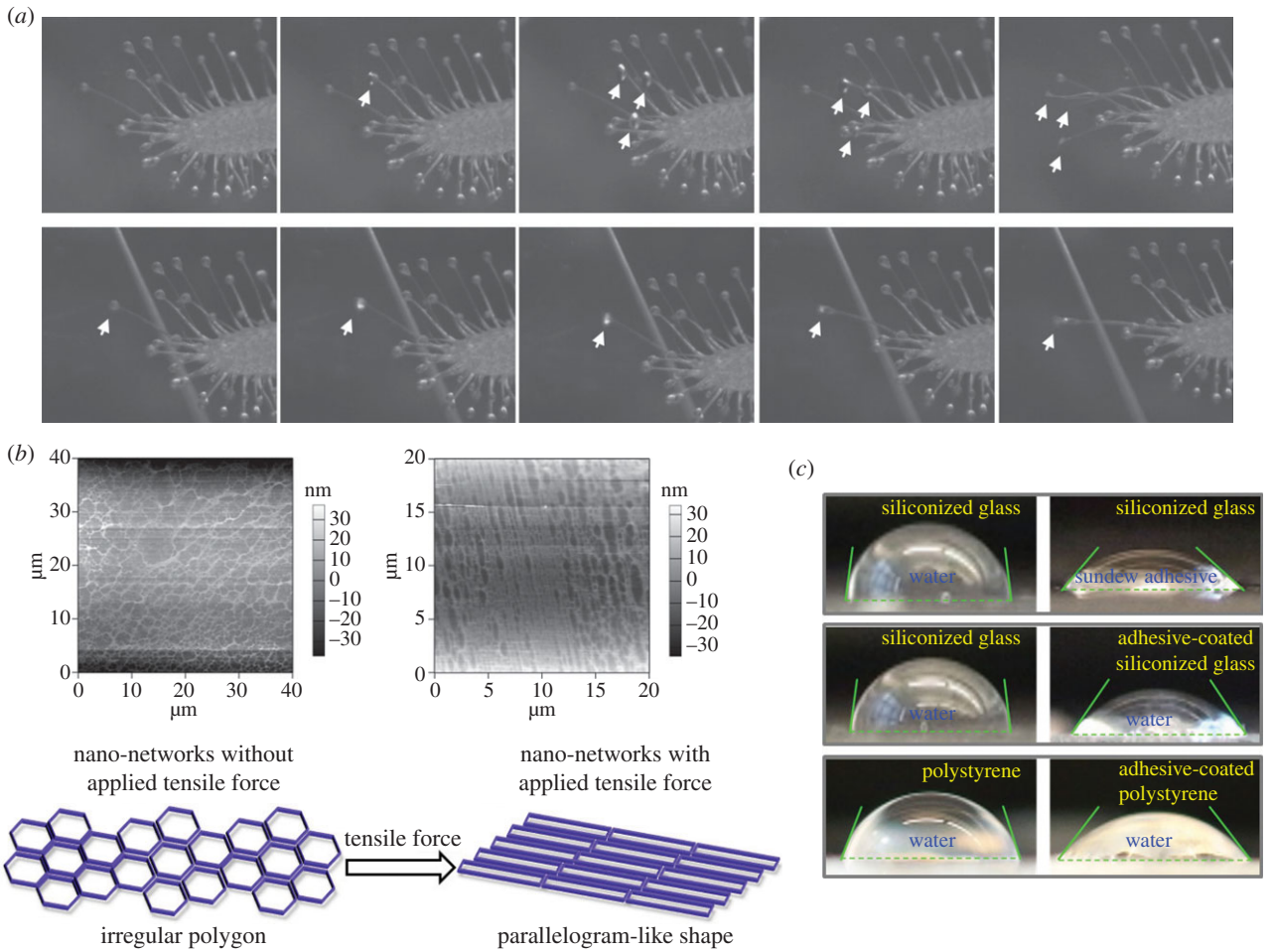

Figure 4. Characterization of the sundew adhesive. (*a*) Images captured by the high-speed camera system (Powerview HS-650), demonstrating the viscoelastic adhesion of sundew adhesive. Microscope coverslips were *in situ* in contact with the adhesive droplets on the leaves of sundew plants. Arrows indicate the flat discs formed by sundew adhesive upon touching the substrates. (*b*) Upper panel, AFM images of the nano-network architectures in sundew adhesive before (left) and after (right) a tensile force was applied. Image sizes are 40 × 40 μm (left) and 20 × 20 μm (right), with height bars. Bottom panel, a schematic drawing of the deformation of the nano-network structures within sundew adhesive, in response to the exerted external force. (*c*) CA measurements. Upper panel, water and sundew adhesive were dropped onto respective siliconized glass slides. Middle panel, water was dropped onto bare siliconized glass slides and sundew adhesive-coated siliconized glass slides, respectively. Bottom panel, water was dropped onto bare polystyrene slides and sundew adhesive-coated polystyrene slides, respectively. (Online version in colour.)

Table 1. CA measurements.

substrate	bare siliconized glass	adhesive-coated siliconized glass[c]	bare polystyrene	adhesive-coated polystyrene[c]
adhesive CA ($CA_{sundew\ adhesive}$)[a]	46.8 ± 1.8°*	—	—	—
water CA (CA_{water})[b]	82.7 ± 1.4°	56.5 ± 2.3°*	70.2 ± 0.9°	53.4 ± 2.7°**

[a]$CA_{sundew\ adhesive}$ was measured via dropping 20 μl of sundew adhesive onto the substrates.
[b]CA_{water} was measured via dropping 20 μl of water onto the respective substrates.
[c]Five microlitres of the sundew adhesive was coated onto the surface of the siliconized glass slide and the polystyrene slide, respectively, and air-dried.
Significant differences between sample means are indicated: *$p < 0.05$, versus the CA_{water} of the bare siliconized glass; **$p < 0.05$, versus the CA_{water} of the bare polystyrene.

changing the surface wettability of hydrophobic substrates via surface coating.

3.5. Sundew adhesive, susceptible to temperature variation

In terms of the dynamic process for the failure of the adhesive, the previous mechanical study has proposed that sundew adhesive resembles one type of industrial glues, i.e. pressure-sensitive adhesive [3]. In most cases, pressure-sensitive adhesives reduce or lose their stickiness at low temperatures due to the decrease in the flexibility and the increase in the hardness/stiffness [46,47]. It is thus reasonable to assume that sundew adhesive may also be susceptible to low temperatures. To test this hypothesis, a pilot study was carried out by measuring the maximum extension

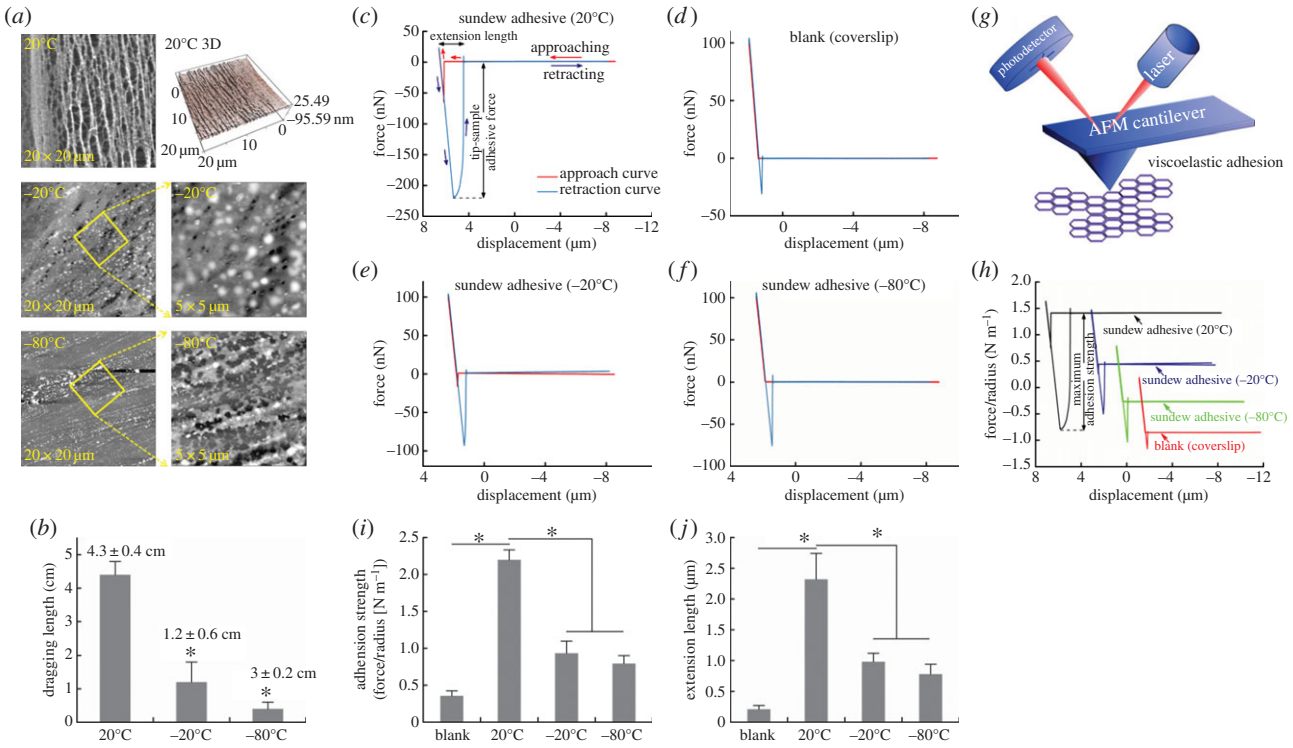

Figure 5. Influence of low temperatures on the performance of sundew adhesive. (*a*) AFM images of the nano-network structures within the sundew adhesives treated at various ambient temperatures. External tensile forces were applied on sundew adhesives prior to the AFM measurements. Upper panel, room temperature (20°C), image sizes are 20 × 20 μm. Middle panel, −20°C, image sizes are 20 × 20 μm (left) and 5 × 5 μm (right). Bottom panel, −80°C, image sizes are 20 μm × 20 μm (left) and 5 μm × 5 μm (right). (*b*) The maximum elongation lengths of sundew adhesives treated at different ambient temperatures. Error bars indicate s.d.; *$p < 0.05$, versus the sundew adhesive treated at room temperature (20°C). Force curves of bare coverslip (*d*) and sundew adhesives treated at 20°C (*c*), −20°C (*e*) and −80°C (*f*) were measured using AFM. (*g*) A schematic drawing of the force curve measurement performed by AFM. (*h*) The adhesion strength (N m^{-1}) versus displacement (μm) curves for sundew adhesives treated at various ambient temperatures were converted from respective force curves. (*i*) Adhesion strengths of sundew adhesives treated at different ambient temperatures. Error bars indicate s.d.; *$p < 0.05$. (*j*) Maximum extension lengths of sundew adhesives treated at distinct temperatures, as measured by AFM. Error bars indicate s.d.; *$p < 0.05$. (Online version in colour.)

length of 20 μl of sundew adhesive that was placed on the coverslips and treated with distinct ambient temperatures, i.e. room temperature, −20°C or −80°C, for 2 h. The adsorbed sundew adhesive was stretched by a needle and the elongation length was recorded upon failure of the adhesive. As shown in figure 5*b*, the maximal elongation of the sample treated at room temperature was approximately 3.6-fold longer than that of the adhesive treated at −20°C, and approximately 14-fold greater than that of the −80°C-treated sample. This substantially diminished extensional capability of sundew adhesive seems to be related to the lowering of ambient temperatures. To further validate this result, the influence of low temperatures on the performance of sundew adhesive was precisely assessed by measuring the adhesion strengths and the extension lengths of the adhesives treated with various ambient temperatures, using AFM (figure 5*g*). For such purpose, the force curves for the samples that were treated at respective temperatures were created according to a method that has been developed for investigating other bioadhesives in the previous studies [14–19]. As shown in figure 5*c–f*, four stages of the interactions between the tip of the cantilever and the adsorbed sundew adhesive were recorded. Initially, force is absent at the interface while the tip of the cantilever approaches the adhesive. A resistance force arises upon touching the adhesive. The value of this force rises with further indentation and declines with the retraction of the cantilever. Upon failure of the adhesive, the retraction curve overlaps with the approach curve, indicating the terminus of the entire force curve measurement. The adhesion strengths for samples treated with different temperatures were calculated, and it was observed that sundew adhesive placed at room temperature exhibited substantially greater adhesion strength than those treated at −20°C or −80°C (figure 5*h*). As shown in figure 5*i*, an adhesion strength of 2.197 ± 0.135 N m^{-1} was obtained in the sundew adhesive treated with room temperature. By contrast, the adhesion strengths for samples treated at −20°C or −80°C were less than 0.95 N m^{-1}. This result well agrees with that of the pilot study mentioned above and further supports the proposed concept that sundew adhesive is susceptible to low temperatures. Apart from the adhesion strength, the extension lengths of the sundew adhesives treated with respective temperatures were also measured via AFM. Information gained from the obtained force curves indicated that the adhesive treated at room temperature showed a maximum extension length of 2.32 ± 0.42 μm, which is substantially greater than those of the samples treated at lower temperatures (0.98 ± 0.14 μm at −20°C, 0.78 ± 0.16 μm at −80°C) (figure 5*j*). The variation trend of the extension lengths of sundew adhesive, in response to the temperature changes, is consistent with the trend of the adhesion strengths. The morphological features of the nano-network architectures within sundew adhesives that were placed at various temperatures were further investigated using AFM, providing insight into the implied mechanisms. As shown in figure 5*a*, for the sundew adhesives treated at

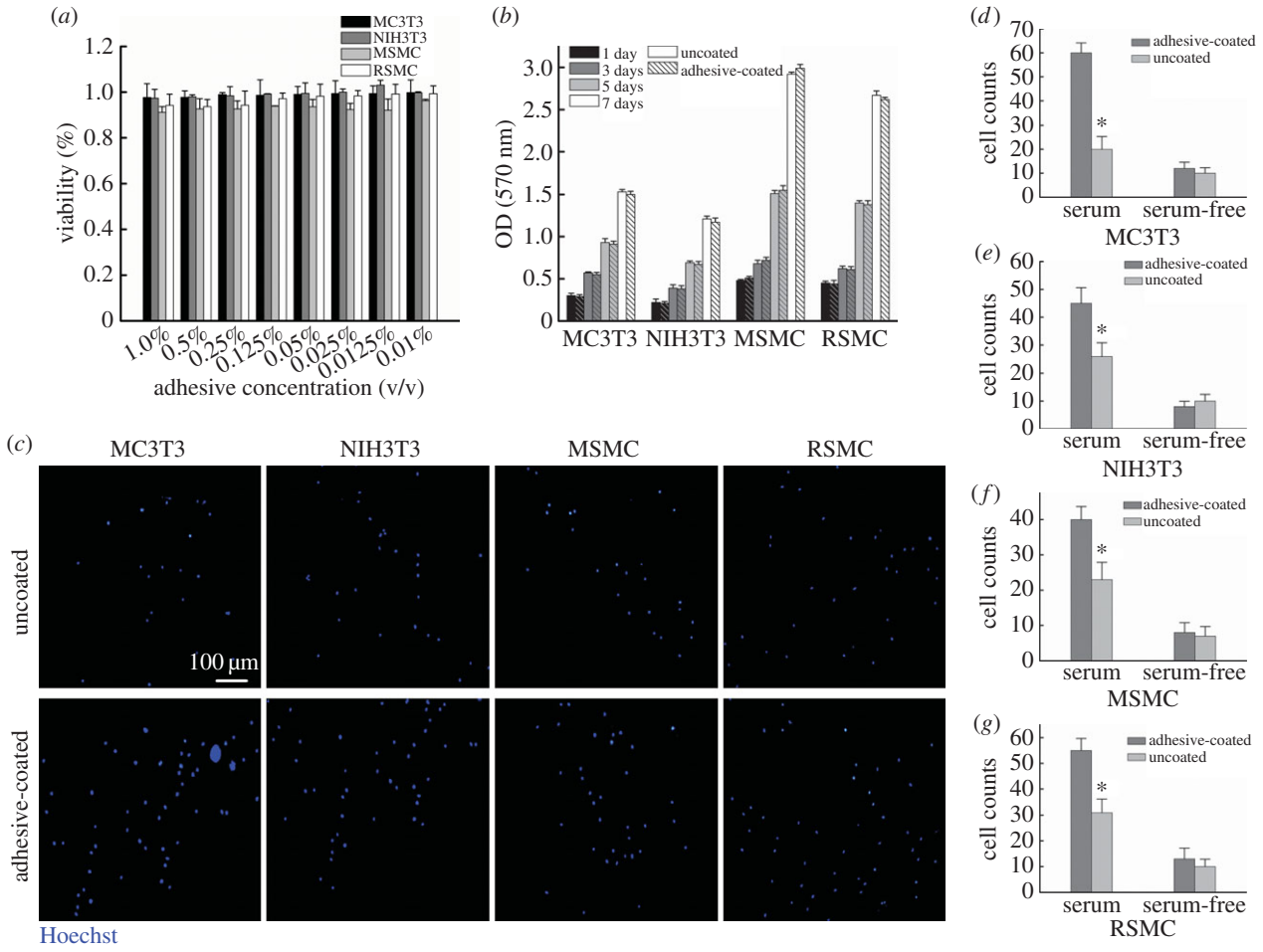

Figure 6. Application of sundew adhesive for tissue engineering. (*a*) MTT assay on sundew adhesive. The cell viabilities were determined as compared to the untreated group. Error bars indicate s.d. (*b*) Cell proliferation tests. Error bars indicate s.d. (*c*) Fluorescent images of the cell adhesion assay in the presence of serum. The nuclei of adherent cells were stained with Hoechst 33342. Scale bar represents 100 μm for all images. (*d*–*g*) Cell adhesion assays. Adherent cells were counted by ImageJ. Error bars indicate s.d. Significant differences between sample means are indicated: $*p < 0.05$, versus the bare coverslips. (Online version in colour.)

−20°C or −80°C, the nanofibres within the tight-knit nano-networks were observed to be fractured into tiny pieces. On the contrary, the nano-networks were well maintained in the sundew adhesive treated at room temperature. The structural fracture in samples treated at subzero temperatures is presumably due to the formed ice crystals, which influence the cross-linked nano-networks within sundew adhesive. This structural fracture eventually impairs the performance of sundew adhesive.

3.6. Sundew adhesive: biocompatible scaffolds for tissue engineering

Apart from the physico-chemical properties characterized above, the potential to exploit sundew adhesive as tissue engineering scaffolds was further investigated in this study. For such a purpose, the biocompatibility of this naturally occurring nanomaterial was thoroughly assessed.

Several cell types that are commonly used for bone/liver/vascular tissue engineering were used to test the cytotoxicity of sundew adhesive, including two types of fibroblast cells, MC3T3 mouse pre-osteoblastic cells [48] and NIH3T3 mouse embryo fibroblast cells [49], as well as two types of smooth muscle cells, MSMCs and RSMCs [50]. As shown in figure 6*a*, apparent cytotoxic activity was not observed in sundew adhesive against these four types of cells and even at a high concentration of sundew adhesive up to 1% (v/v), the inhibition ratios were still less than 8% for all types of cells tested in this study. This result suggests that sundew adhesive possesses good compatibility with common mammal cells. The long-term cytotoxic effect of sundew adhesive was also examined via investigating the proliferation rates of these four types of cells on the scaffolds obtained from sundew adhesive. Consistently, sundew adhesive did not exhibit obvious long-term cytotoxicity towards these types of cells, as no significant difference in proliferation rates was observed between the cells seeded on the scaffolds derived from sundew adhesive and those seeded on the bare TCPs, throughout the 7-day test period (figure 6*b*).

In addition to the evaluated cytotoxicity, the cell adhesion assay was also performed to explore the potential of sundew adhesive to be used for tissue engineering, using four types of cells as mentioned above. As shown in figure 6*c*, it is notable that the scaffolds derived from sundew adhesive are capable of strengthening the adhesion of four types of cells in the presence of serum. In comparison to the bare coverslips, the attachment of MC3T3 on the adhesive-coated substrates was approximately threefold stronger, while approximately 1.7-fold greater attachments of NIH3T3, MSMC and RSMC were obtained on the surfaces modified with sundew adhesive (figure 6*d*–*g*). Interestingly, the enhanced cell adhesion behaviour was not observed in the serum-free condition (figure 6*d*–*g*). Given that cell adhesion activity is a function associated with the density of the binding ligands (proteins or peptides)

adsorbed on the substrates [24,51–54], the elevated cell adhesion on the substrates modified with sundew adhesive in the serum-containing medium presumably arises from the presence of more binding sites provided by the adsorbed serum proteins. Thus, the sundew adhesive strengthens the adsorption of serum proteins and eventually favours cell adhesion.

Apart from these beneficial characteristics demonstrated by sundew adhesive, as a naturally occurring hydrogel, the nano-networks within sundew adhesive render a three-dimensional architecture capable of delivering growth factors, transplanting or implanting cells, presenting stimuli and many others, making it an excellent candidate for developing biocompatible scaffolds in tissue engineering. Moreover, the viscoelastic behaviour allows the sundew adhesive to be a promising candidate for space-filling agents, with the capability of being implanted for directing the growth of tissues [55].

4. Conclusion

To summarize, in this study, the mucilage secreted by sundew plants is identified as a naturally occurring hydrogel. The nano-networks observed within sundew adhesive are structurally flexible, a property that is associated with the viscoelastic behaviour of sundew adhesive. The adhesion strength and the extension length of sundew adhesive are susceptible to low temperatures, which impair the nano-network architectures within sundew adhesive. Finally, the feasibilities of using the nano-networks derived from sundew adhesive as potential scaffolds for tissue engineering are explored. The results indicate that the sundew adhesive is highly biocompatible and capable of intensifying the adhesion of multiple mammal cells owing to the enhanced adsorption of serum proteins. Overall, this study might open a totally new frontier for exploiting sundew adhesive as biocompatible hydrogel in the biomedical field.

Acknowledgements. We thank Benjamin E. Reese for his assistance on AFM characterization and we also thank Juchuan Li for his assistance on XPS measurements in the Oak Ridge National Laboratory.

Funding statement. This research was sponsored by the National Science Foundation (CMMI: 1300167).

Conflict of interests. The authors declare no competing financial interest.

References

1. Adlassnig W, Lendl T, Peroutka M, Lang I. 2010 Deadly glue-adhesive traps of carnivorous plants. In *Biological adhesive systems: from nature to technical and medical application* (eds J Von Byern, I Grunwald), pp. 15–28. Vienna, Austria: Springer. (doi:10.1007/978-3-7091-0286-2_2)
2. Ellison AM. 2006 Nutrient limitation and stoichiometry of carnivorous plants. *Plant Biol.* **8**, 740–747. (doi:10.1055/s-2006-923956)
3. Erni P, Varagnat M, Clasen C, Crest J, McKinley GH. 2011 Microrheometry of sub-nanolitre biopolymer samples: non-Newtonian flow phenomena of carnivorous plant mucilage. *Soft Matter* **7**, 10 889–10 898. (doi:10.1039/c1sm05815k)
4. Šamaj J, Blehová A, Repčák M, Ovečka M, Bobák M. 1999 *Drosera* species (sundew): *in vitro* culture and the production of plumbagin and other secondary metabolites. In *Medicinal and aromatic plants XI* (ed. YPS Bajaj), pp. 105–135. Springer.
5. Gowda D, Reuter G, Schauer R. 1982 Structural features of an acidic polysaccharide from the mucin of *Drosera binata*. *Phytochemistry* **21**, 2297–2300. (doi:10.1016/0031-9422(82)85194-7)
6. Gowda D, Reuter G, Schauer R. 1983 Structural studies of an acidic polysaccharide from the mucin secreted by *Drosera capensis*. *Carbohydr. Res.* **113**, 113–124. (doi:10.1016/0008-6215(83)88223-8)
7. Aspinall GO, Puvanesarajah V, Reuter G, Schauer R. 1984 Selective cleavage of β-d-glucopyranosiduronic acid linkages in methylated polysaccharide acids from *Drosera* species. *Carbohydr. Res.* **131**, 53–60. (doi:10.1016/0008-6215(84)85403-8)
8. Rost K, Schauer R. 1977 Physical and chemical properties of the mucin secreted by *Drosera capensis*. *Phytochemistry* **16**, 1365–1368. (doi:10.1016/S0031-9422(00)88783-X)
9. Gorb S, Voigt D, Gorb E. 2007 Visualisation of small fluid droplets on biological and artificial surfaces using the cryo-SEM approach. In *Modern research and educational topics in microscopy* (eds A Méndes-Vilas, J Diaz), pp. 812–819. Badajoz, Spain: Formatex.
10. Zhang M, Lenaghan SC, Xia L, Dong L, He W, Henson WR, Fan X. 2010 Nanofibers and nanoparticles from the insect capturing adhesive of the sundew (*Drosera*) for cell attachment. *J. Nanobiotechnol.* **8**, 20. (doi:10.1186/1477-3155-8-20)
11. Lenaghan S, Serpersu K, Xia L, He W, Zhang M. 2011 A naturally occurring nanomaterial from the sundew (*Drosera*) for tissue engineering. *Bioinspir. Biomim.* **6**, 046009. (doi:10.1088/1748-3182/6/4/046009)
12. Chase MW, Christenhusz MJ, Sanders D, Fay MF. 2009 Murderous plants: Victorian gothic, Darwin and modern insights into vegetable carnivory. *Bot. J. Linn. Soc.* **161**, 329–356. (doi:10.1111/j.1095-8339.2009.01014.x)
13. Emre Y, Imhof BA. 2014 Matricellular protein CCN1/CYR61: a new player in inflammation and leukocyte trafficking. *Semin. Immunopathol.* **36**, 253–259. (doi:10.1007/s00281-014-0420-1)
14. Callow J, Crawford S, Higgins M, Mulvaney P, Wetherbee R. 2000 The application of atomic force microscopy to topographical studies and force measurements on the secreted adhesive of the green alga *Enteromorpha*. *Planta* **211**, 641–647. (doi:10.1007/s004250000337)
15. Lee H, Scherer NF, Messersmith PB. 2006 Single-molecule mechanics of mussel adhesion. *Proc. Natl Acad. Sci. USA* **103**, 12 999–13 003. (doi:10.1073/pnas.0605552103)
16. Higgins MJ, Crawford SA, Mulvaney P, Wetherbee R. 2002 Characterization of the adhesive mucilages secreted by live diatom cells using atomic force microscopy. *Protist* **153**, 25–38. (doi:10.1078/1434-4610-00080)
17. Crawford SA, Higgins MJ, Mulvaney P, Wetherbee R. 2001 Nanostructure of the diatom frustule as revealed by atomic force and scanning electron microscopy. *J. Phycol.* **37**, 543–554. (doi:10.1046/j.1529-8817.2001.037004543.x)
18. Fang HH, Chan K-Y, Xu L-C. 2000 Quantification of bacterial adhesion forces using atomic force microscopy (AFM). *J. Microbiol. Methods* **40**, 89–97. (doi:10.1016/S0167-7012(99)00137-2)
19. Razatos A, Ong Y-L, Sharma MM, Georgiou G. 1998 Molecular determinants of bacterial adhesion monitored by atomic force microscopy. *Proc. Natl Acad. Sci. USA* **95**, 11 059–11 064. (doi:10.1073/pnas.95.19.11059)
20. Ducker WA, Senden TJ, Pashley RM. 1992 Measurement of forces in liquids using a force microscope. *Langmuir* **8**, 1831–1836. (doi:10.1021/la00043a024)
21. Biggs S, Mulvaney P. 1994 Measurement of the forces between gold surfaces in water by atomic force microscopy. *J. Chem. Phys.* **100**, 8501–8505. (doi:10.1063/1.466748)
22. Sader JE, Chon JW, Mulvaney P. 1999 Calibration of rectangular atomic force microscope cantilevers. *Rev. Sci. Instrum.* **70**, 3967–3969. (doi:10.1063/1.1150021)
23. Sader JE, Larson I, Mulvaney P, White LR. 1995 Method for the calibration of atomic force microscope cantilevers. *Rev. Sci. Instrum.* **66**, 3789–3798. (doi:10.1063/1.1145439)

24. Huang Y, Zhang S, Niu B, Wang D, Wang Z, Feng S, Xu H, Kong D, Qiao M. 2013 Poly(ε-caprolactone) modified with fusion protein containing self-assembled hydrophobin and functional peptide for selective capture of human blood outgrowth endothelial cells. *Colloids Surf. B* **101**, 361–369. (doi:10.1016/j.colsurfb.2012.06.034)
25. Wang Y, Sun L, Yi S, Huang Y, Lenaghan SC, Zhang M. 2013 Naturally occurring nanoparticles from *Arthrobotrys oligospora* as a potential immunostimulatory and antitumor agent. *Adv. Funct. Mater.* **23**, 2175–2184. (doi:10.1002/adfm.201202619)
26. Ahmed EM. 2015 Hydrogel: preparation, characterization, and applications. *J. Adv. Res.* **6**, 105–121. (doi:10.1016/j.jare.2013.07.006)
27. Hamidi M, Azadi A, Rafiei P. 2008 Hydrogel nanoparticles in drug delivery. *Adv. Drug Deliv. Rev.* **60**, 1638–1649. (doi:10.1016/j.addr.2008.08.002)
28. Messersmith PB, Textor M. 2007 Nanomaterials: enzymes on nanotubes thwart fouling. *Nat. Nanotechnol.* **2**, 138–139. (doi:10.1038/nnano.2007.51)
29. Li X, Chang W-C, Chao YJ, Wang R, Chang M. 2004 Nanoscale structural and mechanical characterization of a natural nanocomposite material: the shell of red abalone. *Nano Lett.* **4**, 613–617. (doi:10.1021/nl049962k)
30. Pasqui D, De Cagna M, Barbucci R. 2012 Polysaccharide-based hydrogels: the key role of water in affecting mechanical properties. *Polymers* **4**, 1517–1534. (doi:10.3390/polym4031517)
31. Yang X, Bakaic E, Hoare T, Cranston ED. 2013 Injectable polysaccharide hydrogels reinforced with cellulose nanocrystals: morphology, rheology, degradation, and cytotoxicity. *Biomacromolecules* **14**, 4447–4455. (doi:10.1021/bm401364z)
32. Braccini I, Pérez S. 2001 Molecular basis of Ca^{2+}-induced gelation in alginates and pectins: the egg-box model revisited. *Biomacromolecules* **2**, 1089–1096. (doi:10.1021/bm010008g)
33. Li L, Fang Y, Vreeker R, Appelqvist I, Mendes E. 2007 Reexamining the egg-box model in calcium–alginate gels with X-ray diffraction. *Biomacromolecules* **8**, 464–468. (doi:10.1021/bm060550a)
34. Panouillé M, Larreta-Garde V. 2009 Gelation behaviour of gelatin and alginate mixtures. *Food Hydrocoll.* **23**, 1074–1080. (doi:10.1016/j.foodhyd.2008.06.011)
35. Silva MAd, Bierhalz ACK, Kieckbusch TG. 2009 Alginate and pectin composite films crosslinked with Ca^{2+} ions: effect of the plasticizer concentration. *Carbohydr. Polym.* **77**, 736–742. (doi:10.1016/j.carbpol.2009.02.014)
36. Lotfabad EM, Ding J, Cui K, Kohandehghan A, Kalisvaart WP, Hazelton M, Mitlin D. 2014 High-density sodium and lithium ion battery anodes from banana peels. *ACS Nano* **8**, 7115–7129. (doi:10.1021/nn502045y)
37. Blankschien MD, Pretzer LA, Huschka R, Halas NJ, Gonzalez R, Wong MS. 2012 Light-triggered biocatalysis using thermophilic enzyme–gold nanoparticle complexes. *ACS Nano* **7**, 654–663. (doi:10.1021/nn3048445)
38. Ström A, Ribelles P, Lundin L, Norton I, Morris ER, Williams MAK. 2007 Influence of pectin fine structure on the mechanical properties of calcium–pectin and acid–pectin gels. *Biomacromolecules* **8**, 2668–2674. (doi:10.1021/bm070192r)
39. Gasperini L, Mano JF, Reis RL. 2014 Natural polymers for the microencapsulation of cells. *J. R. Soc. Interface* **11**, 20140817. (doi:10.1098/rsif.2014.0817)
40. Chtchigrovsky M, Lin Y, Ouchaou K, Chaumontet M, Robitzer M, Quignard F, Taran F. 2012 Dramatic effect of the gelling cation on the catalytic performances of alginate-supported palladium nanoparticles for the Suzuki–Miyaura reaction. *Chem. Mater.* **24**, 1505–1510. (doi:10.1021/cm3003595)
41. Schuster E, Eckardt J, Hermansson A-M, Larsson A, Lorén N, Altskär A, Ström A. 2014 Microstructural, mechanical and mass transport properties of isotropic and capillary alginate gels. *Soft Matter* **10**, 357–366. (doi:10.1039/C3SM52285G)
42. Liu Z, Jiao Y, Wang Y, Zhou C, Zhang Z. 2008 Polysaccharides-based nanoparticles as drug delivery systems. *Adv. Drug Delivery Rev.* **60**, 1650–1662. (doi:10.1016/j.addr.2008.09.001)
43. Myrick JM, Vendra VK, Krishnan S. 2014 Self-assembled polysaccharide nanostructures for controlled-release applications. *Nanotechnol. Rev.* **3**, 319–346. (doi:10.1515/ntrev-2012-0050)
44. Xie M, Olderøy MØ, Andreassen J-P, Selbach SM, Strand BL, Sikorski P. 2010 Alginate-controlled formation of nanoscale calcium carbonate and hydroxyapatite mineral phase within hydrogel networks. *Acta Biomater* **6**, 3665–3675. (doi:10.1016/j.actbio.2010.03.034)
45. Zahoor A, Sharma S, Khuller G. 2005 Inhalable alginate nanoparticles as antitubercular drug carriers against experimental tuberculosis. *Int. J. Antimicrob. Agents* **26**, 298–303. (doi:10.1016/j.ijantimicag.2005.07.012)
46. Benedek I. 2004 *Pressure-sensitive adhesives and applications*. Philadelphia, PA: Taylor and Francis.
47. Benedek I, Feldstein MM. 2008 *Applications of pressure-sensitive products*. Philadelphia, PA: Taylor and Francis.
48. Murphy CM, Haugh MG, O'Brien FJ. 2010 The effect of mean pore size on cell attachment, proliferation and migration in collagen–glycosaminoglycan scaffolds for bone tissue engineering. *Biomaterials* **31**, 461–466. (doi:10.1016/j.biomaterials.2009.09.063)
49. Seo S-J, Kim I-Y, Choi Y-J, Akaike T, Cho C-S. 2006 Enhanced liver functions of hepatocytes cocultured with NIH 3T3 in the alginate/galactosylated chitosan scaffold. *Biomaterials* **27**, 1487–1495. (doi:10.1016/j.biomaterials.2005.09.018)
50. Bourget J-M, Gauvin R, Larouche D, Lavoie A, Labbé R, Auger FA, Germain L. 2012 Human fibroblast-derived ECM as a scaffold for vascular tissue engineering. *Biomaterials* **33**, 9205–9213. (doi:10.1016/j.biomaterials.2012.09.015)
51. Veleva AN, Heath DE, Cooper SL, Patterson C. 2008 Selective endothelial cell attachment to peptide-modified terpolymers. *Biomaterials* **29**, 3656–3661. (doi:10.1016/j.biomaterials.2008.05.022)
52. Irvine DJ, Hue K-A, Mayes AM, Griffith LG. 2002 Simulations of cell-surface integrin binding to nanoscale-clustered adhesion ligands. *Biophys. J.* **82**, 120–132. (doi:10.1016/S0006-3495(02) 75379-4)
53. Lee H, Rho J, Messersmith PB. 2009 Facile conjugation of biomolecules onto surfaces via mussel adhesive protein inspired coatings. *Adv. Mater.* **21**, 431–434. (doi:10.1002/adma.200801222)
54. Wei Q, Becherer T, Mutihac R-C, Noeske P-LM, Paulus F, Haag R, Grunwald I. 2014 Multivalent anchoring and cross-linking of mussel-inspired antifouling surface coatings. *Biomacromolecules* **15**, 3061–3071. (doi:10.1021/bm500673u)
55. Drury JL, Mooney DJ. 2003 Hydrogels for tissue engineering: scaffold design variables and applications. *Biomaterials* **24**, 4337–4351. (doi:10.1016/S0142-9612(03)00340-5)